Available online at www.sciencedirect.com
SCIENCE DIRECT
Continental Shelf Research 26 (2006) 1496–1518
CONTINENTAL SHELF RESEARCH
www.elsevier.com/locate/csr

# Circulation and thermal structure in Lake Huron and Georgian Bay: Application of a nested-grid hydrodynamic model

Jinyu Sheng[a,*], Yerubandi R. Rao[b]

[a]Department of Oceanography, Dalhousie University, Halifax, NS, Canada B3H 4J1
[b]Environment Canada, National Water Research Institute, 867 Lakeshore Road, Burlington, Ont., Canada L7R 4A6

Available online 22 June 2006

**Abstract**

A nested-grid hydrodynamic modelling system is used to study circulation and temperature distributions in Lake Huron (LH) and adjacent areas. This nested system is based on the three-dimensional, primitive-equation $z$-level ocean model. The nested system consists of two sub-components: a coarse-resolution outer model covering LH and Georgian Bay (GB) with a horizontal resolution of roughly 2.5 km, and the fine-resolution inner model covering eastern LH and northwestern GB with a horizontal resolution of roughly 900 m. Both the outer and inner models have 30 $z$-levels in the vertical. To assess the model performance, we simulate the three-dimensional circulation and temperature distributions of LH and GB in 1974–1975 and compare the model results with observations made in the lake. We demonstrate that outer model of the nested system simulates reasonably well the large-scale circulation and seasonal evolution of thermal stratifications in LH and GB, and the inner model produces reasonably well the three-dimensional flow and thermal structure over the coastal boundary layer close to the eastern shore of the lake.


*Keywords:* Lake Huron; Seasonal circulation; Thermal structure; Nested-grid model; Coastal jet; Coastal boundary layer

## 1. Introduction

Bordered by the province of Ontario and the state of Michigan, Lake Huron (LH) is the second largest Laurentian Great Lake and the fifth largest freshwater lake in the world. LH contains 3540 $km^3$ of water at low water datum and has a horizontal dimension of about 330 km east to west and 295 km north to south, with a maximum water depth of about 230 m and an average water depth of about 60 m. The most dominant topographic feature in LH is a ridge of Niagaran Dolomite that extends from Thunder Bay, Michigan on the west side, across the lake to Point Clark, Ontario on the east side (Fig. 1), separating the lake into the southwestern and eastern basins. LH comprises four interconnected water bodies: the Main Lake, Saginaw Bay, the North Channel and Georgian Bay (GB), and the lake is connected to Lake Michigan via the Straits of Mackinac (SM) to the northwest, Lake Superior via St. Mary's River (SMR) to the north, and Lake St. Clair via the St. Clair River (SCR) to the south (Fig. 1). Major inflows to LH come from Lake Superior via SMR (about 2100 $m^3 s^{-1}$) and Lake Michigan via SM (about 1400 $m^3 s^{-1}$). LH discharges at its southern end

*Corresponding author. Tel.: +1 902 494 2718; fax: +1 902 494 2885.
*E-mail address:* Jinyu.Sheng@Dal.Ca (J. Sheng).

0278-4343/$ - see front matter © 2006 Elsevier Ltd. All rights reserved.
doi:10.1016/j.csr.2006.01.019

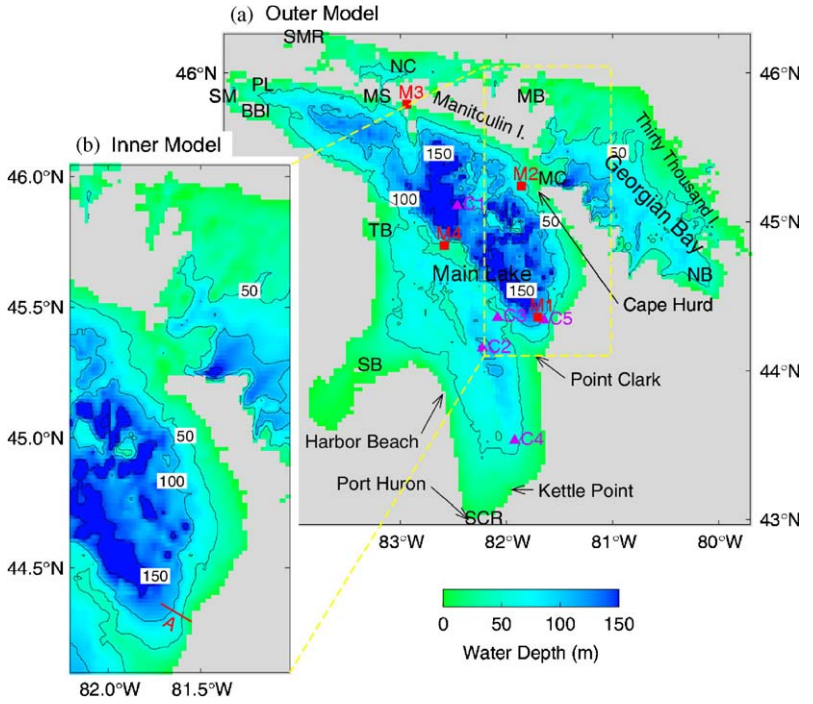


Fig. 1. Selected bathymetric features within the domain of (a) the coarse-resolution outer model, and (b) the fine-resolution inner model of the nested-grid modelling system for Lake Huron and Georgian Bay. Abbreviations are used for St. Mary's River (SMR), St. Clair River (SCR), straits of Macinac (SM), Patrick Landing (PL), Bois Blanc Island (BBI), Mississagi Strait (MS), Main Channel (MC), North Channel (NC), Thunder Bay (TB), Saginaw Bay (SB), Nottawasaga Bay (NB),and Manitowaning Bay (MB). Meteorological and oceanographic observations were made in 1974–1975 at locations marked by solid squares and triangles. Inner model results along transect A are presented in Figs. 5 and 6.

through the SCR into Lake St. Clair, which in turn discharges through the Detroit River into Lake Erie.

The LH ecosystem, which consists of fresh-water fisheries, wildlife, shoreline marshes and wetlands, has been significantly affected by natural and anthropogenic activities. The lake ecosystem is affected by degradation and loss of historical habitat in tributaries and coastal wetlands, invasion of non-native nuisance species such as zebra mussel, over-fishing and wildlife reproduction failure, toxic contaminants and eutrophication in some localized areas. Water use and related water quality problems, particularly from nutrient releases from fish farming, could also impact on the LH ecosystem as the lake water ultimately drains into the North Channel and GB system. LH is now recovering from decades of environmental contamination, but is still threatened by shoreline development and invasive species. Knowledge of water movements and temperature distributions in the lake, interconnected channels and bays will, therefore, be particularly useful to improve the current understanding of the chemical and biological processes that occur simultaneously in the lake.

Early experimental studies on the large-scale circulation in LH were made by Harrington (1894), who observed a prevailing cyclonic surface circulation in the main basin based on trajectories of near-surface drift bottles released in the lake. Sloss and Saylor (1975) analysed the current meter records from 1966 summer moorings and confirmed the general cyclonic circulation during the summer season. As part of the Upper Lakes Reference Study in 1974–1975, several current-meter and temperature moorings were deployed by the Canada Centre for Inland Waters and the Great Lakes Environmental Research Laboratory (IJC, 1977; Saylor and Miller, 1979). Previous observations suggested that the winter mean circulation in the lake is characterized by a southward flow along the west coast and a return northward flow along the east coast. It was also suggested that the region's summer mean circulation is relatively weaker than the winter mean circulation. Another notable feature of the LH summer circulation is a surface flow into GB

that implies a return flow at deeper depths (Saylor and Miller, 1979). Except for these large-scale hydrodynamic experiments, LH has otherwise not received much attention in last 30 years, particularly in the experimental study of thermal structure and hydrodynamics.

Csanady (1968, 1971, 1972a) was the first to theoretically study the baroclinic circulation and associated coastal jets in a circular lake under a suddenly imposed wind forcing based upon the reduced gravity, shallow water equations. Simons (1974) was the first to develop a three-dimensional (3D) hydrodynamic model for the Great Lakes. Beletsky et al. (1999) estimated the mean circulation in the Great Lakes (including LH) from current observations made in the region during the 1960s–1980s. Schwab and Bedford (1994) developed an experimental Great Lakes forecasting system using a 3D terrain-following (or sigma-level) ocean circulation model known as the Princeton Ocean Model (POM). In another application for an idealized lake, Beletsky et al. (1997) compared a $z$-level model performance with the POM. Their results did not show significant differences between these two models. Schwab and Beletsky (2003) recently studied the effects of wind forcing, topography and stratification on the lake-wide circulation in Lake Michigan using the POM.

LH has a complicated basin containing many small islands, shoals, and troughs associated with a glacial scour origin. Accurate numerical simulation of water movements and thermal structure in LH is crucial for development of water quality models for small embayments of the North Channel and GB. In regions of steep bathymetry, however, a sigma-level model may suffer from problems with large numerical errors in calculating the horizontal pressure gradient terms, and a $z$-level model may suffer from problems of a crude steplike representation of the slope bottom topography. Several numerical methods, such as the weighted density Jacobian scheme suggested by Song (1998) and the pressure Jacobian scheme suggested by Shchepetkin and McWilliams (2003), have been developed to improve the numerical accuracy of the pressure gradient terms in the sigma-level model. To improve the $z$-level model performance over the steep bottom topography, Adcroft et al. (1997) suggested a shaved cell (or partial cell) technique, Killworth and Edwards (1999) developed a turbulent boundary layer model, and Song and Chao (2000) proposed an embedded bottom boundary layer formulation. Nevertheless, more accurate simulations using either the sigma-level or the $z$-level models can be obtained by increasing horizontal and vertical resolutions. For an example, Xing and Davies (2001) demonstrated that their sigma-level model with a horizontal resolution of about 3 km is capable to resolve the formation of thermal fronts and associated 3D circulation in the Irish Sea. The main objectives of this study are twofold: to simulate the large-scale circulation, thermal structure and associated seasonal variability in LH and adjacent GB and the North Channel using a nested-grid hydrodynamic modelling system; and to assess the model performance of the nested-grid system by comparing the model results with the observed currents and temperature distributions of 1974–1975. In this study, the nested-grid hydrodynamic modelling system based on the $z$-level ocean circulation model known as CANDIE (Sheng et al., 1998) is used to simulate the 3D circulation and temperature distributions in LH in 1974–1975. As the secondary objective, the model results presented in this paper are used to demonstrate the utility of this $z$-level ocean circulation model in simulating thermal structure and 3D hydrodynamics in lakes using climatic forcing.

The arrangement of this paper is as follows. Section 2 discusses the nested-grid modelling system developed for LH and GB. Section 3 discusses the external forcing used to simulate the lake circulation in 1974–1975. Section 4 presents the model results and comparison of model results with observations made in LH. Section 5 provides a summary and discussion.

## 2. The nested-grid hydrodynamic modelling system

The nested-grid modelling system used in this study is based on the 3D primitive equation $z$-level ocean circulation model known as CANDIE (Canadian version of DieCAST, Sheng et al., 1998). CANDIE has been successfully applied to various modelling problems on the continental shelf seas, including wind-driven circulation over an idealized coastal canyon (Sheng et al., 1998), a density-driven coastal current (Sheng, 2001), tidal circulation in the Gulf of St. Lawrence (Lu et al., 2001), wind-driven circulation over a stratified coastal embayment (Davidson et al., 2001), and seasonal circulation in the northwestern Atlantic Ocean (Sheng et al., 2001). Most recently CANDIE has been applied to the western Caribbean Sea by

Sheng and Tang (2003, 2004) and Lunenburg Bay of Nova Scotia by Sheng and Wang (2004) and Wang et al. (2006). The reader is referred to the Appendix for the governing equations used in CANDIE.

The nested-grid modelling system of LH has two sub-components: a coarse-resolution outer model covering LH and GB between 79.4°W and 84.7°W and between 43°N and 46.3°N; and a fine-resolution inner model covering eastern LH and western GB between 81°W and 82.2°W and between 44.1°N and 46.1°N (Fig. 1). The main reason for setting up the inner model over this region is to resolve the detailed 3D currents and temperature distributions through the Main Channel and within the coastal boundary layer close to the eastern shore of the lake. The nested system uses the bathymetry of Schwab and Sellers (1996), with model horizontal resolutions of about 2.5 km and 900 m, respectively for the outer and inner models. Both the outer and inner models have the same 30 unevenly spaced $z$-levels in the vertical, with the centers of each $z$-level located at 1.5, 4.5, 7.5, 10.5, 13.5, 16.5, 19.5, 22.5, 25.5, 28.5, 31.5, 34.5, 37.5, 40.5, 43.5, 50.8, 62.5, 74.2, 85.8, 97.5, 109.2, 120.8, 132.5, 144.2, 155.8, 167.5, 179.2, 190.8, 202.5 and 214.2 m, respectively. The nested system uses the sub-grid scale mixing parameterization scheme of Smagorinsky (1963) for the horizontal eddy viscosity, and the scheme proposed by Large et al. (1994) for the vertical eddy mixing coefficient. The horizontal turbulent Prandtl Number (i.e., the ratio of the horizontal eddy diffusivity coefficient to the horizontal eddy viscosity coefficient) is set to 0.1. The model also uses the fourth-order numerics suggested by Dietrich (1997) and flux limiter suggested by Thuburn (1996) to better represent the nonlinear advection terms in the model momentum and temperature/salinity equations. It should be noted that the mixing scheme of Large et al. (i.e., KPP scheme) was primarily designed to approximate the vertical mixing processes in the ocean interior. For the vertical mixing over coastal and shelf regions, better schemes such as the two-equation turbulence model of Mellor and Yamada (1982) or the one-equation turbulence model of Xing and Davies (1995, 2001) should be used. Durski et al. (2004) modified the KPP scheme by including a bottom boundary layer parameterization to the standard KPP scheme. They demonstrated that model results using their modified KPP scheme compare reasonably well to those using the level-2.5 Mellor–Yamada scheme in series of idealized continental shelf experiments. In this study, the standard KKP scheme is used. The effect of the modified KKP scheme developed by Durski et al. in numerical results in the lake will be examined in the future study.

The outer model of the nested system has three open boundaries (i.e., northern, western and southern open boundaries), with specifications of steady inflows to LH from Lake Superior via SMR ($\sim 2100\,m^3\,s^{-1}$) and Michigan via SM ($\sim 1400\,m^3\,s^{-1}$) and outflows from LH into Lake St. Clair via SCR ($\sim 3500\,m^3\,s^{-1}$). Since gradient boundary conditions are used for temperature fields along the outer model open boundaries, the river runoff specified at the outer model open boundaries plays only a minor role in driving the general circulation in the lake. The currents and temperatures produced by the outer model are used to specify current and temperature distributions at the open boundaries of the inner model (i.e., the conventional one-way nesting, see Sheng et al. (2005)). In addition, the outer and inner models of the nested-grid system use the quadratic bottom friction parameterization with the drag coefficient set to $2.5 \times 10^{-3}$, and the no-slip condition at the model lateral closed boundaries, at which the normal and tangential flows and horizontal fluxes of temperature are set to zero.

## 3. Model external forcing

In addition to the boundary forcing (i.e., currents and temperature along the model open boundaries) described above, two additional model forcings are used to simulate the 3D circulation and thermal structure in the lake in 1974–1975. The first additional model forcing is wind stress applied at the lake surface. Fig. 2a shows the wind stress converted from the observed wind speeds at three meteorological stations M2, M3 and M4 in LH based on the bulk formula suggested by Large and Pond (1981). Since the observed wind stress only covered the period from yearday 135–320 in 1974, we also use the wind stresses converted from 12 hourly wind speeds extracted from the National Centers for Environmental Prediction (NCEP of the National Center for Atmospheric Research) 40-year reanalysis dataset (Kalnay et al., 1996) in this study. In comparison with the observed wind stress, there are two issues in using the NCEP/NCAR wind stress to drive the model. First, the coarse-resolution (147 km × 208 km in LH) NCEP/NCAR wind stress does not reproduce well the spatial

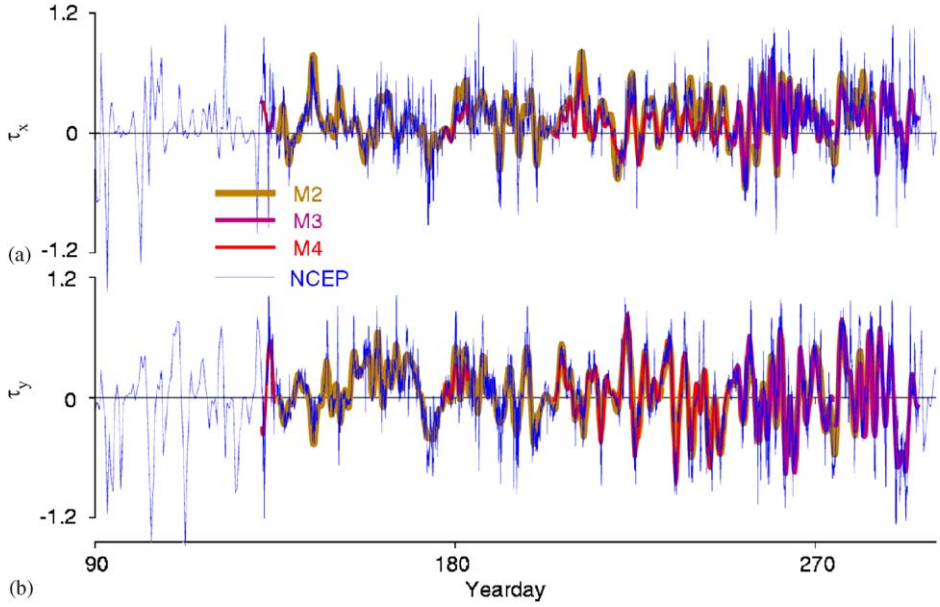


Fig. 2. Time series of the wind stresses converted from observed wind speeds at three locations (M2, M3, and M4) and those calculated from the combination of 12 hourly wind speeds based on the NCEP/NCAR reanalysis and the observed wind at three locations in 1974.

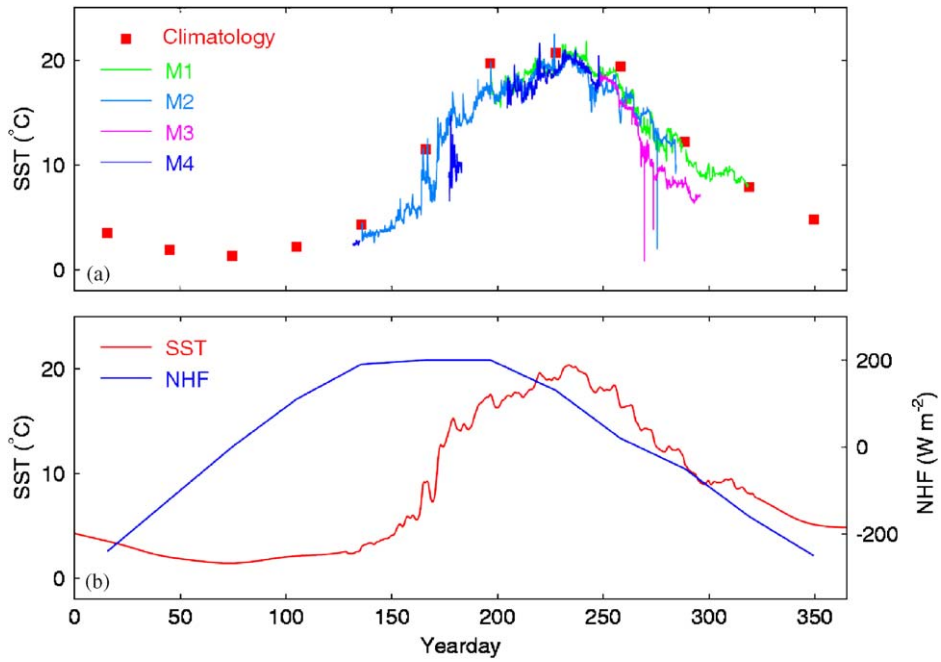


Fig. 3. (a) Comparison of observed lake surface temperature (LST) at four locations in 1974 and climatological monthly mean LST in Lake Huron, and (b) time-series of LST and monthly mean net heat flux (NHF) used to force the nested-grid model. Both the monthly mean LST and NHF were taken from model results computed by the Great Lakes Net Basin Supply Forecast Model (http:mcc.sws.uiuc.edu/glakes/hur/nhu.html).

variabilities of the observed wind stress in LH. Second, the NCEP/NCAR wind stress on average is significantly weaker than the observed wind stress. To improve the representation of the NCEP/NCAR wind forcing in the study region, we spatially average the NCEP/NCAR wind stress in LH and

modify the amplitude of the area-averaged NCEP/NCAR wind stress based on the observed wind stress during the period of yearday 135–320 in 1974 using the least squares fitting method. The modified and area-averaged NCEP/NCAR wind stress (Fig. 2), which is used to drive the nested-grid modelling system, is highly comparable with, and occasionally larger than, the observed wind stress, as expected.

The second additional model forcing is the net heat flux (NHF) at the lake surface ($Q_{net}$) parameterized as:

$$Q_{net} = Q_{net}^{input} + \gamma(LST^{input} - LST^{model}), \quad (1)$$

where $Q_{net}^{input}$ is the input net heat flux (NHF), $LST^{input}$ is the input lake surface temperature 0(LST), $LST^{model}$ is the model-calculated LST, and $\gamma$ is the coupling coefficient defined as $\Delta z_1 \rho_o c_p / \tau$, where $\Delta z_1$ is the thickness of the top $z$-level, $c_p$ is the specific heat, and $\tau$ is the restoring time scale set to 15 days. The implied value of $\gamma$ is about $35\,W\,m^{-2}\,K^{-1}$, which is comparable to values calculated from observations (Haney, 1971). Since there were no NHF observations made in LH during the study period, $Q_{net}^{input}$ is assumed to be horizontally uniform and equal to the climatological monthly mean NHF (Fig. 3(b)) calculated from results produced by the Great Lakes Net Basin Supply Forecast (GLNBSF) Model (http:mcc.sws.uiuc.edu/glakes/hur/nhu.html) for simplicity. Lake surface temperatures were measured at four meteorological stations M1, M2, M3 and M4 in LH but only for the period from yearday 130–320 in 1974 (Fig. 3(a)). As a result, the input LST ($LST^{input}$) used in model simulation is also assumed to be horizontally uniform and equal to the linear combination of observed LST and the climatological monthly mean LST ($LST^{clim}$) calculated from the GLNBSF model results during the above LST observation period (Fig. 3(b)), and equal to $LST^{clim}$ at other times.

It should be noted that the wind stress and net heat flux at the lake surface have significant spatial variability in LH, particularly over the coastal regions (Saylor and Miller, 1979). The influence of spatial variability of these two forcing on the 3D circulation and thermal structure in LH remains to be studied.

## 4. Model results

We initialize the nested-grid hydrodynamic modelling system with a spatially uniform temperature of 4 °C and salinity of 0.2 psu at every model grid point, and force the model with the time-varying and spatially uniform wind stress and net surface heat fluxes described in Section 3. We integrate the nested-grid system for 2 years from 1 January 1974 to the end of 1975. As pointed out by Beletsky and Schwab (2001), the typical spin-up time of the lake circulation is relatively short, due mainly to the strong wind-driven character of the lake hydrodynamics. Therefore, the effect of the initial condition on the long-term model simulation should be negligible after a few weeks.

### 4.1. Monthly mean circulation and thermal structure in 1974

We first examine the monthly mean circulation of 1974 produced by the nested-grid modelling system. The main reason for focusing on the model results in 1974 in this section is that the model forcing is more realistic in this year than in 1975 (see Section 3).

The monthly mean near-surface (at 1.5 m) circulation in February in LH is characterized by spatially variable (in amplitude) and nearly southward currents in the Main Lake, and cyclonic (counter-clockwise) coastal currents near the shore (Figs. 4(a and b)), which is consistent in general with the near-surface circulation patterns in an idealized and stratified lake studied by Csanady (1971, 1972a). Over northwestern LH, the February mean near-surface currents are approximately westward in the eastern and central regions, and veer southwestward over the western region, to form a narrow coastal jet that runs southeastward along the western shoreline from Bois Blanc Island to Saginaw Bay. After passing Saginaw Bay, the coastal jet turns gradually offshore to flow southeastward into southern LH. The southeastward currents merge over the coastal region near Kettle Point and form a narrow coastal jet running northward along the eastern shore of southern LH. The northward coastal jet joins the southeastward currents flowing along the ridge of Niagaran Dolomite, and forms a narrow offshore jet that runs approximately northward along isobaths of about 80 m over the eastern coastal region of LH. Between the narrow offshore jet and the eastern shoreline of LH, there are narrow and approximately southeastward coastal currents (see the inner model results in Fig. 4(a)). In GB, the February mean near-surface currents are

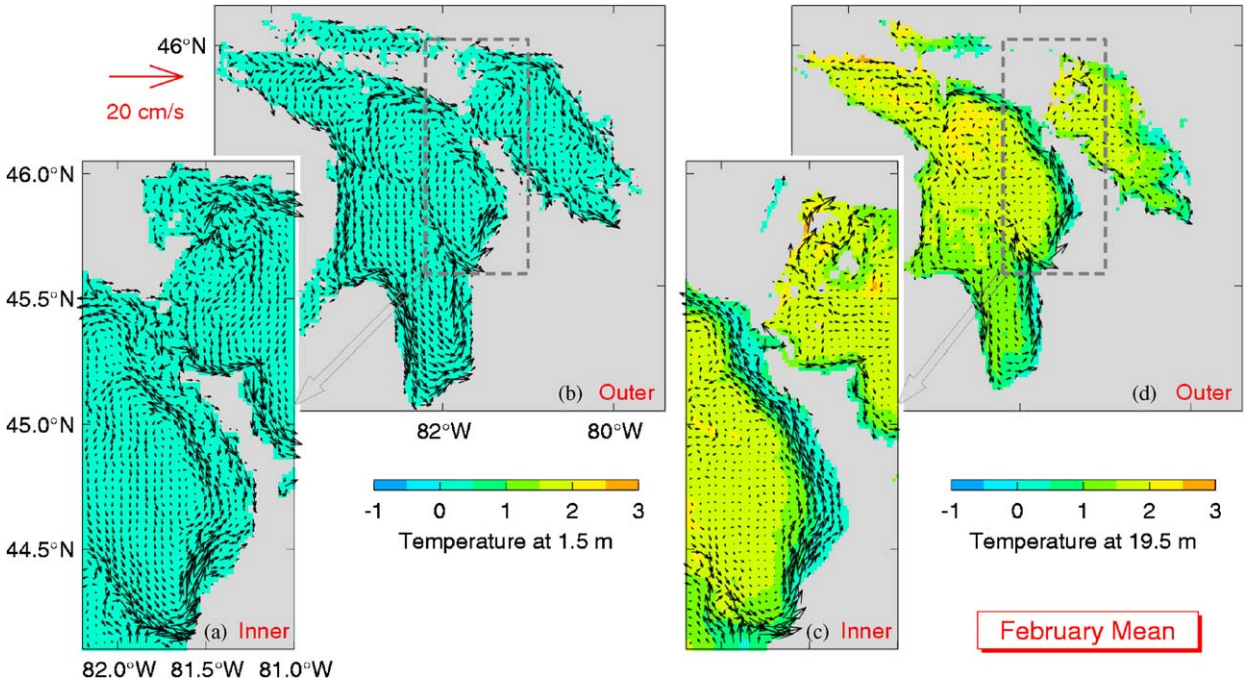


Fig. 4. Monthly mean (a and b) near-surface (1.5 m) and (c and d) sub-surface (19.5 m) currents and temperature distributions in February 1974. Velocity vectors are plotted at every third model grid point for (b and d) outer model results, and at every fourth grid point for (a and c) inner model results.

nearly southwestward over the central region and southeastward (alongshore) over the eastern and western coastal regions.

The February mean sub-surface (19.5 m) circulation in LH and GB is characterized by relatively strong cyclonic currents in western and eastern shallow water regions and relatively weak and spatially variable currents in the deep water regions (Figs. 4(c and d)). The sub-surface currents are also spatially variable, with many small-scale recirculation features over northwestern GB near Manitowaning Bay and southern GB near Nottawasaga Bay.

The February mean near-surface (1.5 m) temperature is horizontally uniform and near the freezing point of 0 °C in LH and GB (Figs. 4(a and b)). The sub-surface (19.5 m) temperature in February is about 2 °C in the deep part of LH and GB and near the freezing point over the shallow regions where the strong coastal currents occur, indicating the importance of baroclinic effects over the coastal regions in February. It should be noted that model-calculated temperature fields in winter months are approximate since a simple parameterization of fresh water ice formation is used in the nested system (i.e., water temperature is set to the freezing point of 0°C if the model-calculated temperature is below the freezing point).

As demonstrated in Fig. 4, the fine-resolution inner model reproduces reasonably well the large-scale circulation features produced by the outer model, and much better the detailed circulation features over the coastal boundary layer (CBL) close to the eastern shoreline of LH, due mainly to a better representation of bottom topography and dynamics within the CBL by the inner model using a finer horizontal resolution than the outer model. (The inner and outer models use the same bottom topography of about 2 km, indicating a similar representation of coastlines of the lake in both the inner and outer models). The CBL comprises a frictional boundary layer (FBL) near the coast and an inertial boundary layer (IBL) offshore (Murthy and Dunbar, 1981). The main difference between the FBL and IBL is that the momentum imparted by the wind stress is balanced by bottom and shore friction within the FBL and balanced by the Coriolis term, bottom friction and pressure gradients within the IBL (Rao and Murthy, 2001). Based on the current meter studies made in summer of 1974 over the coastal region near Point Clark of

Lake Huron (section A in Fig. 1), Murthy and Dunbar (1981) suggested that the FBL and IBL widths are respectively about 2 and 8 km in summer months in LH. Rao and Murthy (2001) suggested the FBL and IBL widths to be about 3 and 5~6 km during summer stratification in Lake Ontario estimated from current observations in a coastal region of Lake Ontario in 1990.

Fig. 5(a) presents vertical distributions of monthly mean along-shore currents at transect A in February 1974 produced by the inner model with a fine horizontal resolution of 900 m. The flow structure along the same transect was studied previously by Murthy and Dunbar (1981) based on the current observations made in 1974. The February mean along-shore currents at the transect are characterized by relatively weak currents at the coast and sea bottom due to the shore and bottom friction, and a surface-intensified strong velocity core of about 9 cm $s^{-1}$ at about 4 km from shore. The center of this high velocity core varies from about 3 km from shore at the surface to 5 km at 30 m depth. The along-shore currents are more vertically uniform in the top 40 m beyond 5 km from shore and decrease to 2–3 cm $s^{-1}$ at 10 km. By choosing the position at which the alongshore currents reach a maximum as the boundary between the FBL and IBL (Murthy and Dunbar, 1981), the FBL width produced by the inner model is about 4 km in February 1994 along transect A. (No attempt is made in this study to estimate the width of the IBL since the definition of the outer boundary for the IBL is less definitive, for instance, Murthy and Dunbar (1981) suggested the outer boundary of the IBL as the position where the inertial oscillation begins to dominate shore-parallel flow, and Rao and Murthy (2001) suggested the outer boundary of the IBL to be the position where the turbulence kinetic energy contributes maximum to the total kinetic energy.)

The February mean temperature along transect A is vertically uniform and colder than 1 °C in the top 15 m and weakly stratified and slightly warmer of 1–3°C below 20 m within the CBL (Fig. 6(a)). Within the IBL, the isotherms tilt to intersect the lake bottom nearly normally. The doming of the thermocline within the IBL can be explained by the fact that the sub-surface water of about 4 °C in the deep part of the lake is mixed upward (Davidson et al., 1998). It should be noted that the detailed flow and thermal structure produced by the inner model has significant spatial variability along the eastern shore of LH (Figs. 4(a and c)).

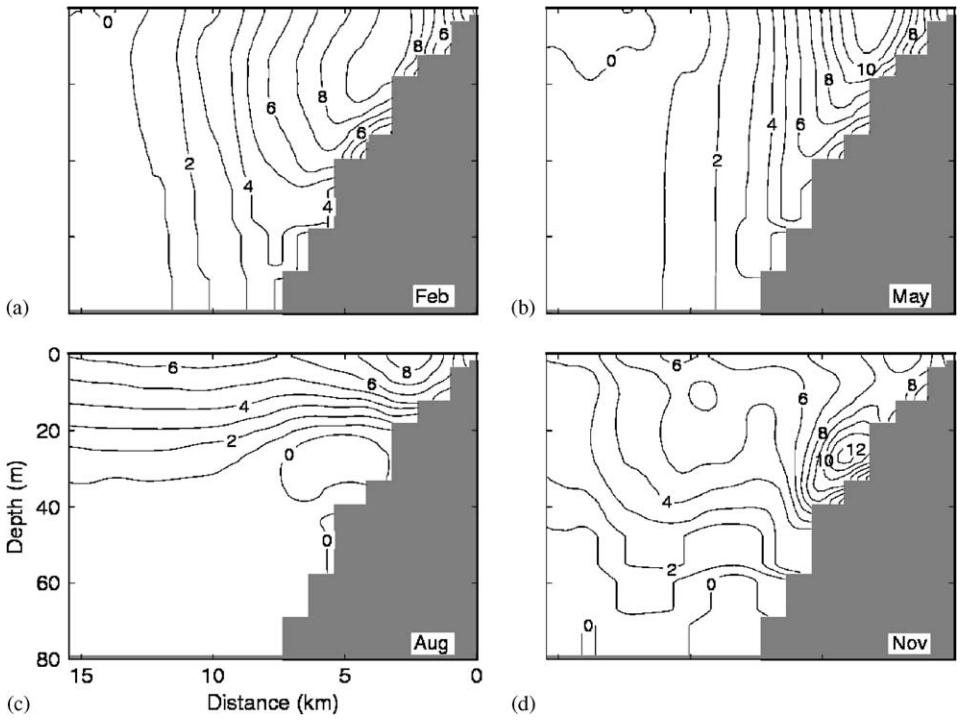


Fig. 5. Vertical distributions of monthly mean along-shore currents in (a) February, (b) May, (c) August, and (d) November of 1974 produced by the high-resolution inner model at transect A shown in Fig. 1.

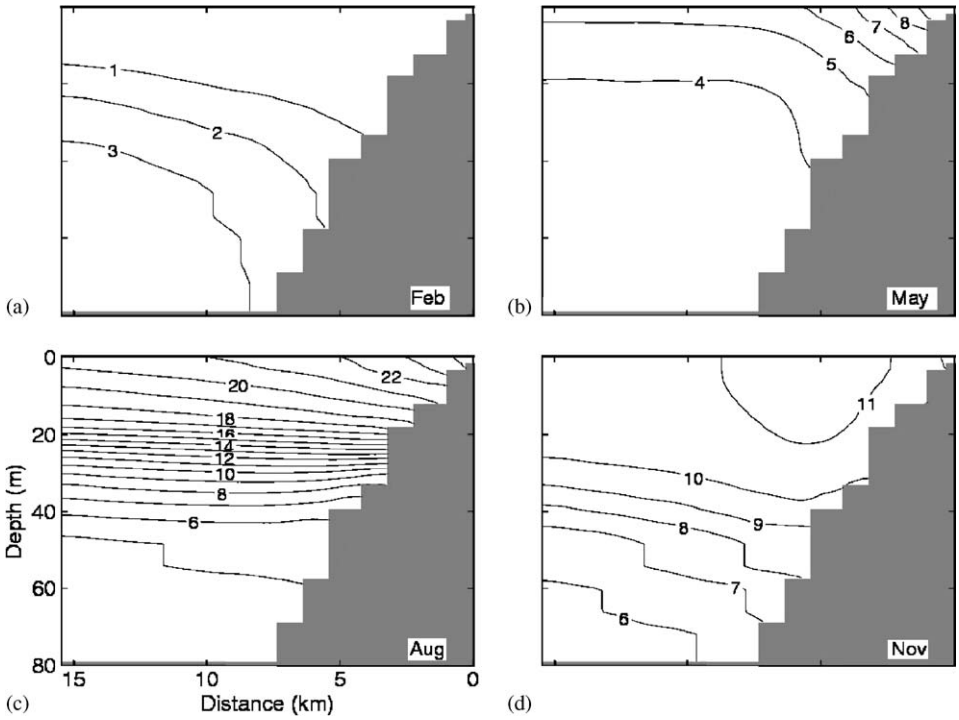


Fig. 6. Vertical distributions of monthly mean temperature in (a) February, (b) May, (c) August, and (d) November of 1974 produced by the fine-resolution inner model at transect A shown in Fig. 1.

The monthly mean near-surface currents in May are characterized by southeastward currents in the Main Lake, and a cyclonic coastal jet flowing southward along the west coast from Bois Blanc Island to Port Huron and then northward along the east coast from Kettle Point to Cape Hurd (Figs. 7(a and b)). There is also an intense anti-cyclonic coastal jet in May, which flows southeastward along the northeastern shoreline from Patrick Landing to the southwestern coastal region of Manitoulin Island. The May mean near-surface currents are approximately southward in GB, except for the southwestern and northwestern coastal regions. The near-surface currents are southeastward (alongshore) over the coastal region near Nottawasaga Bay and southeastward (offshore) over the coastal region near Manitowaning Bay in GB. A comparison of Figs. 4(a) and 7(a) demonstrates that monthly mean near-surface currents in February and May have similar large-scale features in LH and GB, with major differences in small-scale features. The near-surface currents over central LH are approximately southeastward and spatially more uniform in May and southward and spatially less uniform in February. The cyclonic coastal jet is closer to the eastern shore of LH from Kettle Point to Cape Hurd in May than in February.

The sub-surface circulation in May has similar large-scale features as that in February, characterized by relatively strong cyclonic coastal currents along the western and eastern coasts of LH, and relatively weak and highly variable currents over the central regions of LH and GB (Figs. 7(c and d)). In addition, the May mean sub-surface circulation also has a narrow anti-cyclonic coastal jet running southeastward along the northeastern shoreline of LH from Patrick Landing to the western coastal waters of central Manitoulin Island, and highly variable coastal currents over northern GB near Nottawasaga Bay.

Fig. 7 also demonstrates that the near-surface waters in May warm up significantly over the narrow coastal regions close to the shore in LH and GB, with the warmest near-surface temperature of about 12 °C in Saginaw Bay and along coastal regions of Thirty Thousand Islands over eastern GB. In the central regions of LH and GB, the near-surface temperature in May is relatively colder and about 5–6 °C. There are two pools of relatively cold surface waters over the deep waters of the Main

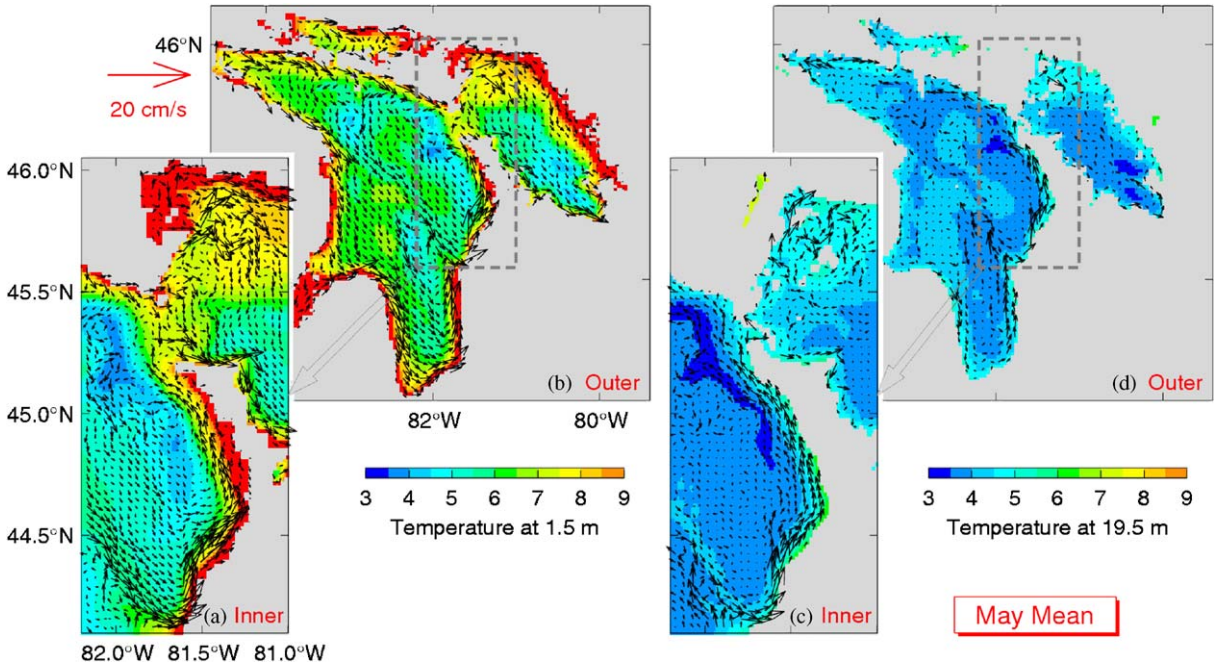


Fig. 7. Monthly mean (a and b) near-surface (1.5 m) and (c and d) sub-surface (19.5 m) currents and temperature distributions in May 1974. Velocity vectors are plotted at every third model grid point for (b and d) outer model results, and at every fourth grid point for (a andc) inner model results.

Lake in May, due mainly to the effect of vertical mixing which brings a significant amount of heat from warmer surface waters to colder sub-surface waters. The May mean sub-surface temperature is relatively uniform and about 4–5 °C in the central regions of LH and GB and relatively warmer and about 6 °C along the narrow coastal regions, except for the northern coastal region where the sub-surface water is relative colder due to coastal upwelling (Figs. 7(a and b)).

The thermal structure and associated cyclonic jet over the FCL shown in Figs. 5(b) and 6(b) demonstrate that the baroclinic dynamics also play an important role over the coastal regions of the lake in May. The May mean along-shore currents at transect A have similar distributions as those in February, except that the along-shore currents are relatively stronger over the FBL in May than in February (Fig. 5(b)). The along-shore currents in May reach a maximum value of about 11 cm $s^{-1}$ at about 3 km from shore, and decrease to about 1 cm $s^{-1}$ at 10 km from shore. The FBL width in May produced by the inner model is about 3 km, which is slightly narrower than in February. Different from the February mean thermal structure along transect A, the May mean thermal structure within the FBL is characterized by inclined isotherms that separate warmer inshore waters of 5–9 °C over the FBL and cold offshore waters of less than 4 °C. Within the IBL, the May mean water temperature is about 4 °C below 20 m, with a weak thermal stratification in the top 20 m due to surface heating in spring. The overall distributions of the thermal structure within the CBL in May shown in Fig. 5(b) agree reasonably well to the observations made by Csanady (1972b) in Lake Ontario in May 1970.

In August, the monthly mean near-surface circulation is characterized by spatially uniform and southeastward currents in the Main Lake, a lake-wide cyclonic gyre in LH, and a bay-wide cyclonic gyre in GB (Figs. 8(a and b)). Similar to the near-surface circulation in February and May, the lake-wide cyclonic gyre in LH in August has an intense coastal jet that flows approximately southward along the western coast from Bois Blanc Island to Harbor Beach, and northward along the eastern coast from Kettle Point to Cape Hurd. The northward coastal jet along the eastern shoreline of LH splits into two branches after passing Cape Hurd, with a small branch turning eastward to flow into GB to form a broad cyclonic coastal jet along

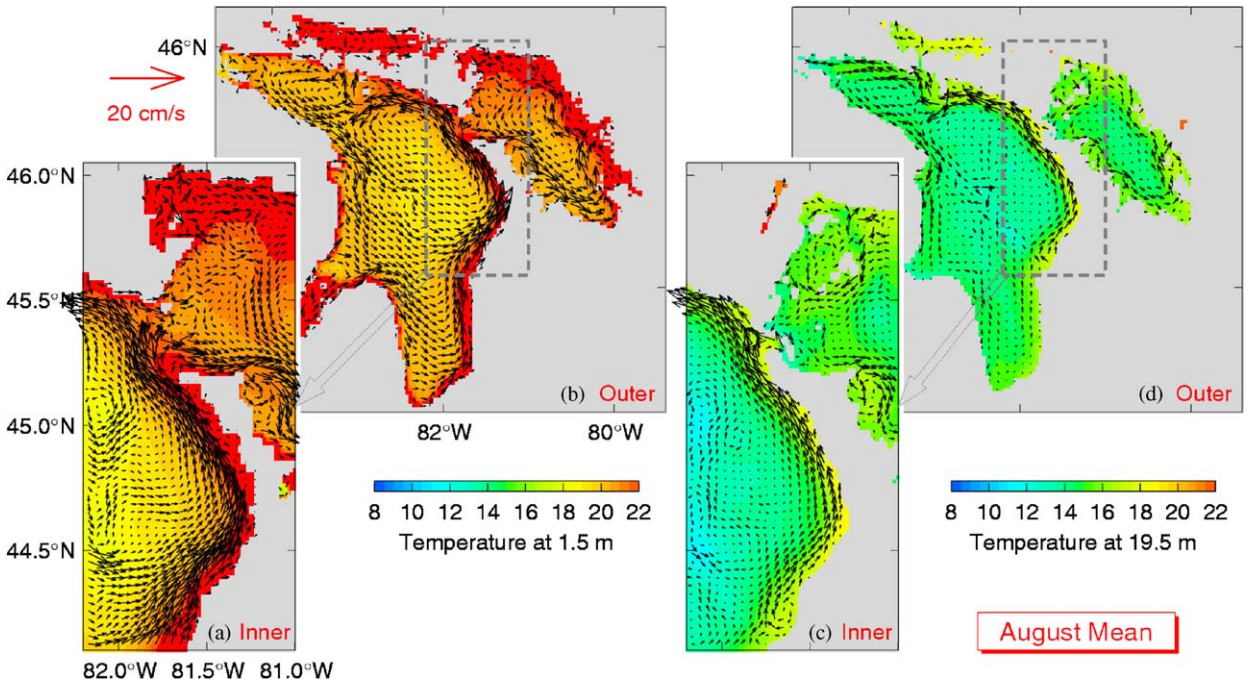


Fig. 8. Monthly mean (a andb) near-surface (1.5 m) and (c andd) sub-surface (19.5 m) currents and temperature distributions in August 1974. Velocity vectors are plotted at every third model grid point for (b andd) outer model results, and at every fourth grid point for (a andc) inner model results.

the western coastal region of GB. The main branch flows northwestward to the western coastal region of Manitoulin Island and veers cyclonically to flow southwestward over the shallow water region between the Main Lake and northern LH. Over northern LH, strong upwelling in the coastal region between straits of Macinac and Patrick Landing leads to intense southeastward (offshore) currents. After leaving the coastal upwelling region, the southeastward currents veer first anti-cyclonically and then cyclonically as reaching the western shore of LH, forming an intense coastal jet to flow southeastward along the western shoreline from Bois Blanc Island to Thunder Bay. The August mean near-surface circulation also has a narrow and intense anti-cyclonic coastal jet that flows southeastward along the eastern shore from Mississagi Strait to the southwest coast of Manitoulin Island, and then runs into Georgian Bay through the northern part of the Main Channel. In GB, the bay-wide cyclonic gyre contains broad and southeastward coastal currents of about $10\,\mathrm{cm\,s^{-1}}$ over western GB from the Main Channel to Nottawasaga Bay, and a return northwestern flow over eastern GB.

The sub-surface (19.6 m) circulation in August is dominated by three interconnected cyclonic gyres in LH and a bay-wide cyclonic gyre in GB (Figs. 8(c and d)). These cyclonic gyres occupy the southwestern, eastern and northwestern basins of LH, respectively. The cyclonic gyre over the southwestern basin is characterized by a coastal jet flowing southward from Thunder Bay to Port Huron, northward from Kettle Point to Point Clark and northwestward along the western flank of the ridge between Point Clark to Thunder Bay. The cyclonic gyre over the eastern basin is characterized by cyclonic currents flowing southeastward along the northeastern flank of the ridge from Thunder Bay to Point Clark, and northward along the eastern shoreline of LH from Point Clark to the coastal region of northwestern Manitoulin Island. The cyclonic currents separate into two branches before reaching the western side of Mississagi Strait, with one branch running westward along the shallow waters between the northwestern and eastern basins and turning cyclonically as reaching the western coast near Thunder Bay. The second branch flows northwestward along the coast from Mississagi Strait to Patrick Landing to form a smaller-size cyclonic gyre over northwestern LH.

The August mean near-surface temperature reaches about 22 °C in the central basin of LH and western GB, and about 25 °C in Saginaw Bay, in the eastern coastal region of LH from Kettle Point to Cape Hurd, and over eastern GB and southern eastern North Channel (Figs. 8(a) and (b)). In comparison, due mainly to the occurrence of intense coastal upwelling (Fig. 8a), the near-surface waters in August are colder along the northern coastal region of LH from Patrick Landing to Mississagi Strait, the western coastal region from Bois Blanc Island to Saginaw Bay, and the coastal region between Harbor Beach and Port Huron of southern LH. The August mean sub-surface temperature is about 12 °C in LH except for the eastern coastal region from Point Clark to Mississagi Strait, where the sub-surface temperature is about 16 °C (Figs. 8c and d). In GB, the sub-surface temperature is about is about 12 °C over the central basin and about 16 °C over the southwestern and eastern coastal regions.

Vertical distributions at transect A of monthly mean currents and temperature in August (Figs. 5(c) and 6(c)) differ significantly from those in February and May, due mainly to strong thermal stratifications in summer months in the lake. The August mean thermal structure at the transect is characterized by a strong thermal stratification in the top 40 m and weak stratification below 60 m, with warmest waters of greater than 22 °C over the inshore region (Fig. 6(c)). The overall distributions of temperatures within the CBL in August produced by the inner model agree reasonably well to the observed thermal structures in the Great Lakes by Csanady (1972b) and Rao and Murthy (2001).

The August mean along-shore currents at transect A are characterized by a near-surface high velocity core of about 8 cm $s^{-1}$ centered at about 3 km from shore and broad, surface-intensified along-shore currents over the offshore region between 10 km and 30 km from shore, The along-shore currents decrease with depth and are very weak below 40 m (Fig. 5(c)). Dynamically, the along-shore currents at the transect are driven primarily by horizontal gradients of baroclinic pressures associated with the summer thermal stratification, the similar physical processes for generating a cyclonic circulation associated with the cold water dome in the northern Irish Sea during the summertime (Xing and Davies, 2001). The August mean FBL width along transect A is about 3 km, which is consistent with the estimates made by Murthy and Dunbar (1981) and Rao and Murthy (2001).

The November mean near-surface currents also have three interconnected cyclonic gyres in LH and a bay-wide cyclonic gyre in GB (Figs. 9(a and b)). The largest cyclonic gyre in LH has similar characteristics as in August, dominated by a broad coastal flow running southward along the western coast, a narrow and intense inshore jet flowing northward along the eastern coast, and narrow southwestward flow along the shallow region between the Main Lake and northwestern basin to close the loop of the gyre. Embedded inside this lake-wide gyre, there is a smaller-size cyclonic gyre in the eastern basin. This smaller-size cyclonic gyre flows northward along the eastern coast from Point Clark to Great Duck Island and then turns southwestward to reach the western coastal region near Thunder Bay. It then flows southeastward along the ridge of Niagaran Dolomite from Thunder Bay to Point Clark to close the loop of the gyre. The smallest cyclonic gyre occurs on the northwestern basin of LH, with a strong southeastward coastal jet over the coastal region near Bois Blanc Island and a return northwestward coastal jet over the coastal region near Mississagi Strait. In GB, the monthly mean near-surface currents in November 1974 have a bay-wide cyclonic gyre in GB, which is also very similar to that in August.

The sub-surface currents in November are very similar to those in August, with three interconnected cyclonic gyres over the northwestern, eastern and northwestern basins of LH and a bay-wide cyclonic gyre in GB (Figs. 9(c and d)). The coastal currents associated with the three gyres in LH are relatively broader and stronger in November than in August. By comparison, the coastal currents in GB are relatively weaker in November than in August.

The near-surface temperature in November is about 9 °C over the deep water regions of LH and GB and about 11 °C over the shallow water regions (Figs. 9(a and b)). Over the narrow coastal regions close the western shore of LH and eastern shore of GB and in Saginaw Bay the near-surface waters are relatively colder and less than 5 °C. The colder inshore waters in November are due mainly to stronger vertical mixing in the month. The sub-surface temperature in November is about 10 °C in the deep water regions and slightly warmer and about 11 °C in the shallow water regions of LH and GB (Figs. 9(c and d)).

The November mean along-shore currents within the FBL at transect A are very similar to those in August, with a near-surface high velocity core of

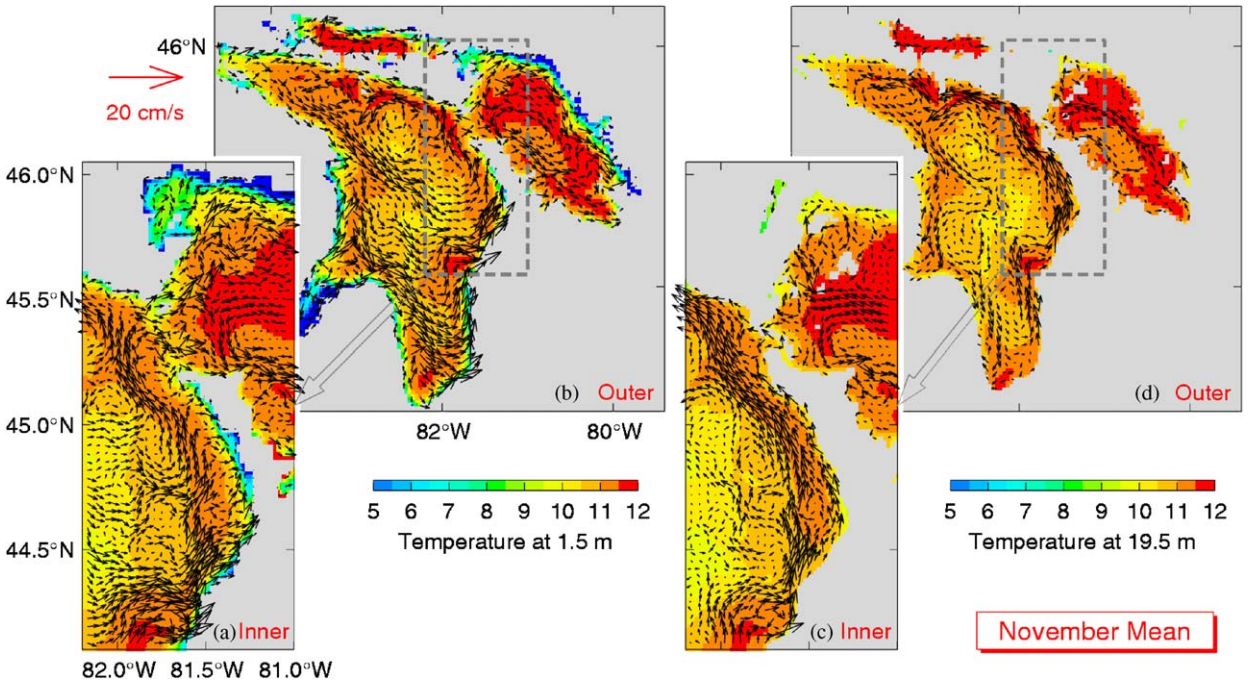


Fig. 9. Monthly mean (a andb) near-surface (1.5 m) and (c andd) sub-surface (19.5 m) currents and temperature distributions in November 1974. Velocity vectors are plotted at every third model grid point for (b andd) outer model results, and at every fourth grid point for (a andc) inner model results.

about 9 cm $s^{-1}$ centered at about 3 km from shore (Fig. 5(d)). Different from the model results in other three months, the November along-shore currents have a sub-surface high velocity core centered at about 30 m from the lake surface at about 4 km from shore. Beyond 10 km from shore, the November along-shore currents at the transect are about 4 to 6 cm $s^{-1}$ in the top 60 m, with many small-scale circulation features (Fig. 5d). The November mean temperature distributions at the transect are vertically uniform in the top 20 m and weakly stratified between 20 and 80 m (Fig. 6d) due to the occurrence of vertical convection in later fall (see Section 4.2 for more discussion).

### *4.2. Seasonal thermal structure and summer mean circulation in 1974–1975*

One of the most important hydrodynamic features in LH is profound seasonal variations of thermal structure that changes from entirely vertically mixed in later fall and early spring to strongly stratified in summer (Boyce et al., 1989). To further demonstrate the performance of the nested-grid modelling system in simulating the seasonal cycle of the thermal structure in LH, we examine the time–depth distributions of simulated temperature fields at four selected sites in Figs. 10 and 11. The main reason for choosing these sites is that current-meter moorings were deployed at these sites in 1974–1975 and comparison of model results with current observations at these sites will be presented in Section 5.

Due to strong vertical convection associated with surface cooling in later fall and early winter in 1974–1975, water temperatures produced by the outer model at sites C1 and C5 (Fig. 10) are vertically homogeneous at about 4 °C, at which the lake water density reaches maximum. The continuous surface cooling in winter months leads to a weak thermal stratification in the top 30 m, with relatively cold waters of 1–3 °C overlying relatively warmer waters of 4 °C in middle winter. Gradual warming in later winter and early spring produces slightly warmer, and therefore denser, waters in the surface layer, leading to strong convection and vertically homogeneous temperature of 4 °C in the lake during this period. The thermal stratification in the upper lake is reestablished in summer due to continuous surface heating, with isotherms of

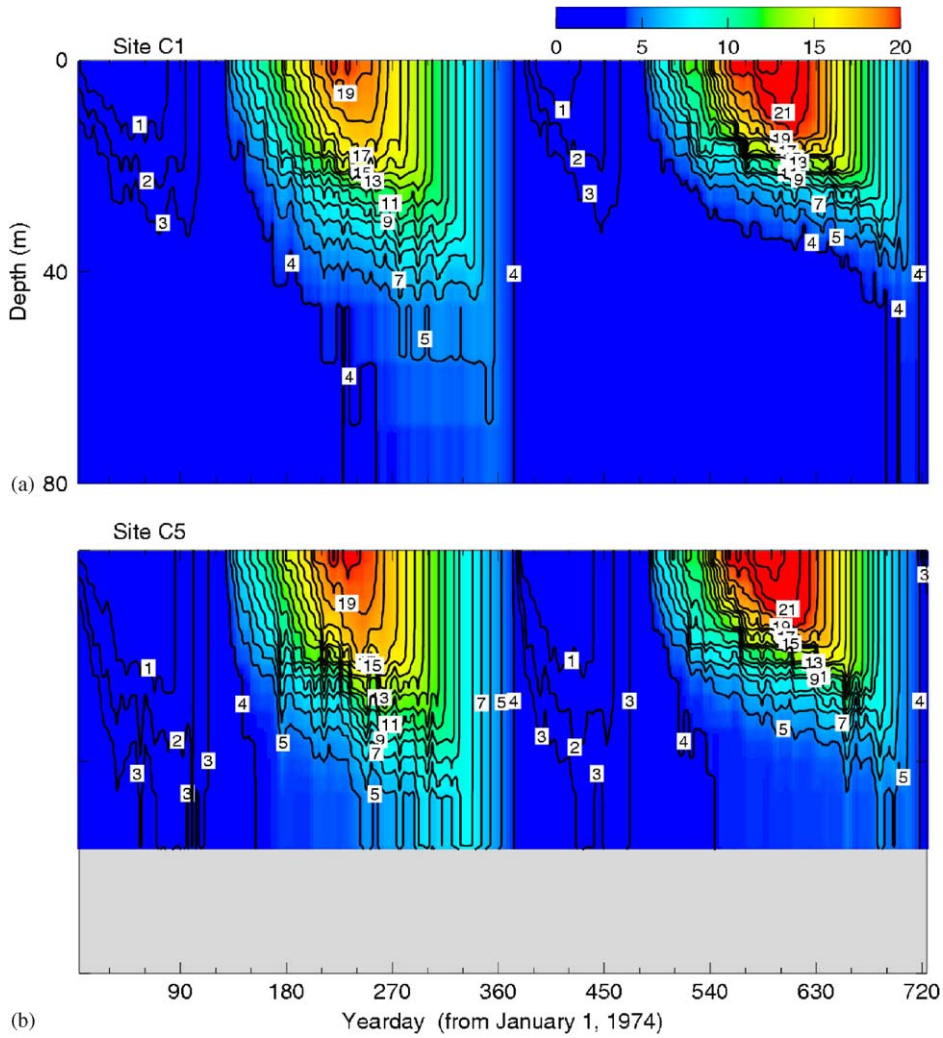


Fig. 10. Time-depth distributions of model calculated temperature for the 2-year period starting from 1 January 1974 to the end of 1975 at sites C1 and C2.

4–10 °C deepening about 30 m from June to September. After the near-surface temperature reaches the maximum value of about 20 °C in middle summer, the thermal stratification of the upper 30 m is gradually erased in fall due to vertical convection triggered by surface cooling. The vertical convection is relatively weak and shallow and reaches about 10 to 20 m in early fall and is much stronger and reaches about 100 m in the deep water regions in later fall and early winter. The simulated thermal structures presented in Fig. 10 are highly comparable to those observed previously in the lake (Saylor and Miller, 1979; Boyce et al., 1989) as well as those produced by Beletsky and Schwab (2001) using a sigma-level model in Lake Michigan. It should be noted that the time-depth evolutions of temperature at four sites in 1975 differ from those in 1974, mainly due to the differences in the model external forcing between the 2 years (Section 3).

Fig. 11 shows the near-surface circulation patters in summer suggested by Sloss and Saylor (1975) based on the current-meter observations made in LH in summer of 1966. The main features of Sloss and Saylor's near-surface currents are characterized by two cyclonic cells in LH, with the largest cell over the Main Lake, which has southward currents along the eastern coast of the lake and return northward currents along the eastern coast, and a smaller-sized cyclonic cell over northwestern LH. The general circulation feature suggested by Sloss and Saylor

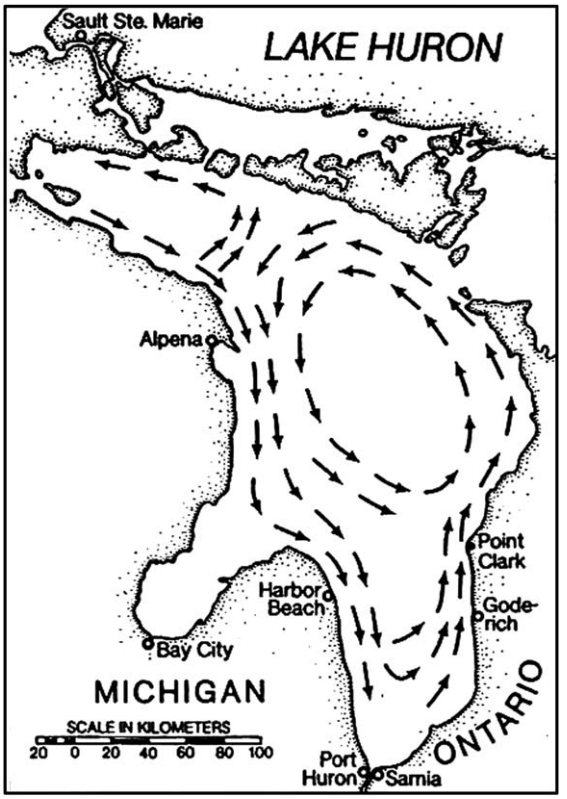


Fig. 11. Schematic diagram of the surface circulation patterns in summer suggested by Sloss and Saylor (1975).

(1975) is similar to that suggested by Harrington (1894) based on trajectories of near-surface bottles in summer months of 1892–1893. Sloss and Saylor (1975) also suggested a persistent surface flow running into GB from LH and subsurface return flow of bay water into the lake through the Main Channel.

To demonstrate the model performance in simulating the seasonal mean circulation in the lake, we calculate the spring and summer mean near-surface circulations from the outer model results in 1974–1975 (Fig. 12). The large-scale patterns of the summer (July–September) mean near-surface currents produced by the outer model (Fig. 12(b)) are similar to Sloss and Saylor's circulation patterns, characterized by a basin-wide cyclonic circulation in LH and bay-wide cyclonic circulation in GB with a inflow from the lake to the bay through the Main Channel. However, significant differences occur between the model results and Sloss and Saylor's circulation patterns. The model-calculated near-surface currents in summer are roughly southeastward and more uniform spatially than Sloss and Saylor's circulation patterns over the central region of the lake. The model-calculated summer mean circulation also has an intense coastal jet that runs southwestward along the west coast of Manitoulin Island. Large differences also occur in Saginaw Bay. The summer mean near-surface circulation produced by the model has northeastward (outward) coastal currents along both the southern and northern shore of Saginaw Bay and southwestward (inward) currents over the central region of the bay. An examination of model results at different depths (not shown) indicates that part of the outflow in the surface layer of Saginaw Bay is provided by the inward flow through the deep channels, which is consistent with previous findings (IJC, 1977).

The seasonal mean near-surface currents produced by the outer model in the other three seasons of winter (January–March, not shown), spring (April–June, Fig. 12(a)) and fall (October–December, not shown) have similar large-scale circulation features as in summer, with a basin-wide cyclonic gyre in the Main Lake and bay-wide cyclonic gyre in Georgian Bay. The simulated seasonal mean near-surface currents have significant seasonal variability. The northward flow along the eastern coast of LH is relatively stronger in winter and summer than in spring and fall. The southeastward flow along the ridge from Thunder Bay to Point Clark is relatively stronger in winter and fall than in spring and fall. The southeastward coastal jet along the western shore of GB is broader and stronger in winter, summer and fall than in spring. In addition, the southeastward coastal jet along the northern coast from Patrick Landing to northwestern shore of Manitoulin Island is relatively stronger in winter and summer and relatively weaker in spring and fall.

### *4.3. Assessing the model performance using current and temperature observations made in 1974–1975*

We first assess the model performance in simulating the monthly mean circulation in LH and compare the monthly mean currents produced by the outer model with the monthly mean current observations made in LH in a five-month period from December 1974 to April 1975. Fig. 13 shows the monthly mean observed currents in three months of December, February and April. Readers are referred to Saylor and Miller (1979) for the monthly mean currents in other 2 months of January and March.

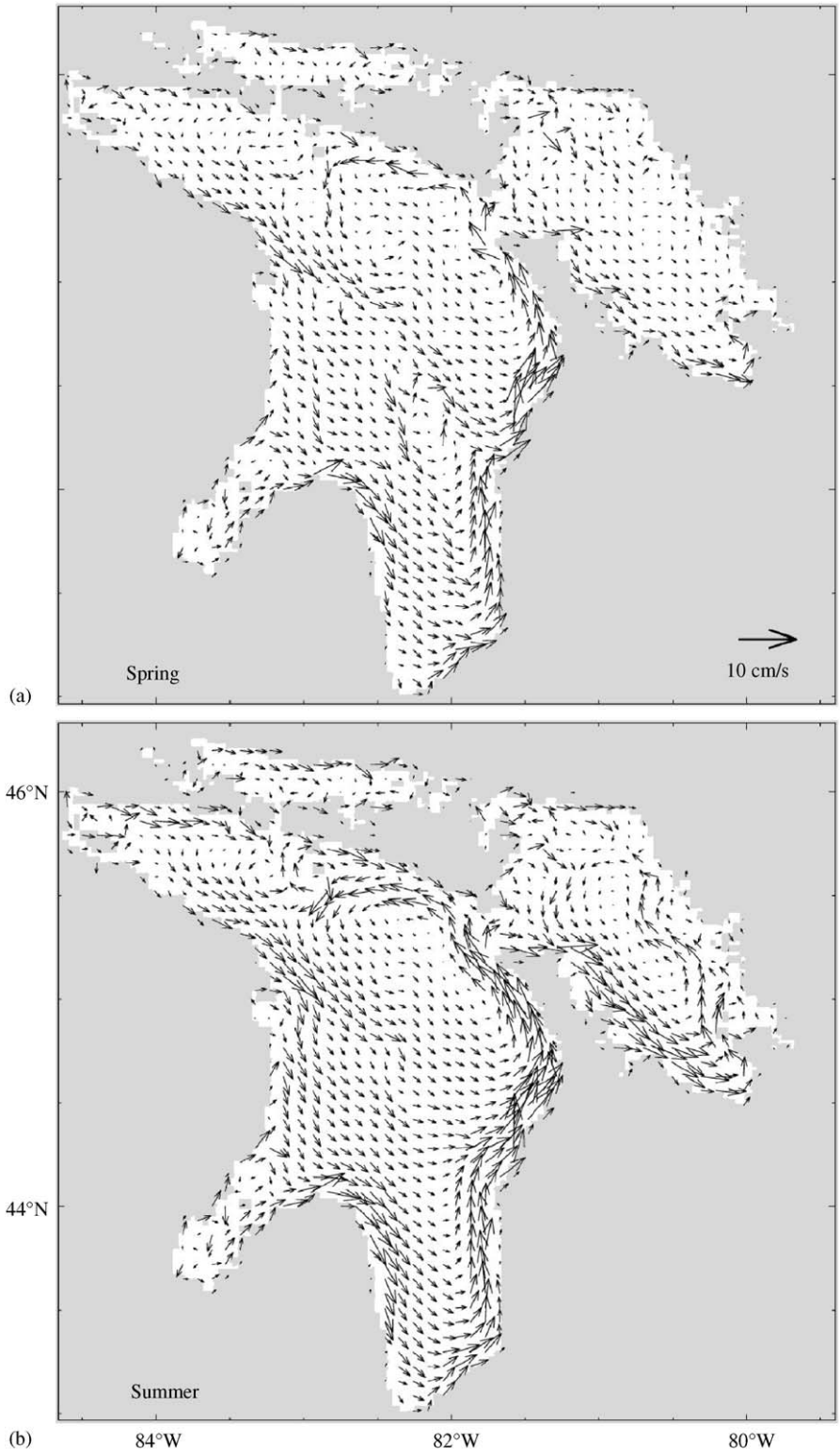


Fig. 12. Seasonal mean near-surface (1.5 m) currents in (a) spring and (b) summer calculated from 2-year model results in 1974–1975. Velocity vectors are plotted at every third model grid point.

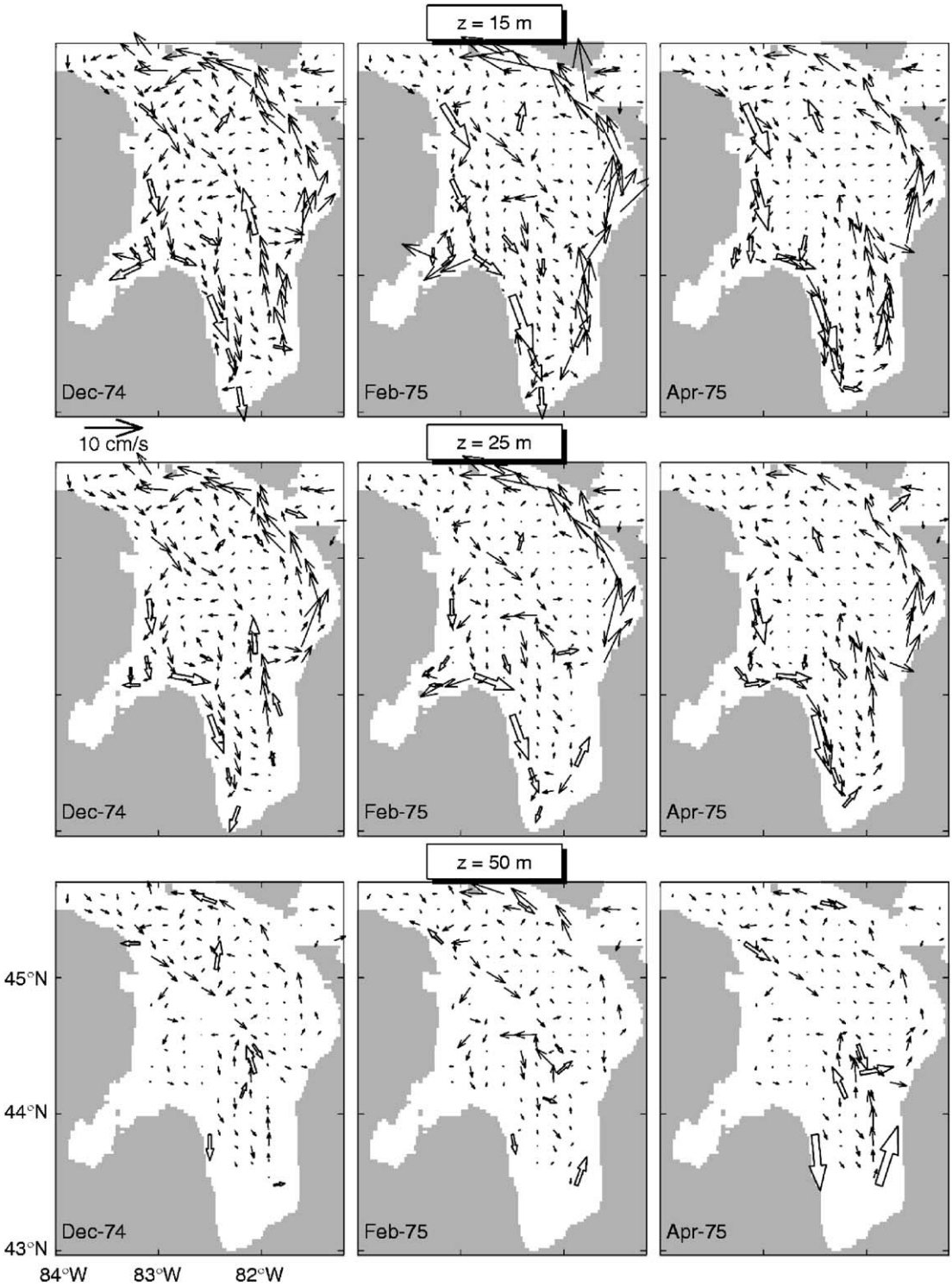


Fig. 13. Comparison of simulated (black arrows) and observed (open arrows) monthly mean currents in 3 months of December (1974), February and April (1975) at depths of 15 m, 25 m, and 50 m, respectively. The simulated currents are produced by the coarse-resolution outer model. Velocity vectors of calculated currents are plotted at every fifth model grid point for clarity.

The nested-grid outer model reproduces reasonably well the general circulation patterns of observed monthly mean currents, particularly the southward currents along the western coast of LH, at depths of 15 m and 25 m in three months of December, March and April. (The model-data comparisons of currents in the three selected months mentioned above are shown in Fig. 13.) The outer model however significantly underestimates the observed southward currents along the western coast of LH in January and February at these two depths. Although the exact reason for large model deficiency at 15 and 25 m is not clear, one possible explanation is that wind forcing used to drive the model (which is assumed to be spatially uniform) is less realistic in January and February than other months. Saylor and Miller (1979) demonstrated that the monthly mean wind forcing was strongest in January with much larger spatial variations than in the other 4 months of 1974–1975. Another possible explanation is associated with the fact that a simple parameterized ice model is used in this study.

The outer model performs reasonably well in reproducing the observed monthly mean currents at 50 m in December, January and February, but less well over the southern LH in March and April. In these 2 months, the outer model reproduces reasonably well the observed currents over the northern and central basins of LH, but much less well in simulating the intense coastal jet flowing cyclonically along the southern coast of LH (Fig. 13).

To quantify the model performance, we calculate the misfit between the observed and simulated monthly mean currents defined as

$$J = \frac{\sum_{k}^{N}[(u_k^o - u_k^s)^2 + (v_k^o - v_k^s)^2]}{\sum_{k}^{N}[(u_k^o)^2 + (v_k^o)^2]}, \quad (2)$$

where $(u_k^o, v_k^o)$ are the horizontal components of the observed currents at the $k$th location estimated by Saylor and Miller (1979), $(u_k^s, v_k^s)$ are the horizontal components of the simulated currents produced by the outer or middle models at the same $k$th location as the observations respectively, and $N$ is the total number of locations where observations were made. The smaller $J$, the better the model results fit the observations. The $J$ value is about 0.49 for the model-observations at 15 m, 0.74 at 25 m and 0.83 at 50 m, indicating that the outer model performance gets worse at deeper depths.

Fig. 14 shows the comparison of the observed monthly mean currents with the monthly mean currents produced by the fine-resolution inner model at the three different depths in the months of December, February and April. Although there are only a small number of observed currents available over the inner model domain, the inner model results reproduces reasonable well the observed monthly mean currents, particularly the currents through the Main Channel and coastal currents over the coastal region near Point Clark, with the $J$ value of about 0.92 and 0.41 at depths of 25 m and 50 m, respectively.

We next assess the model performance in simulating hydrodynamics in LH over frequency bands of a few hours to months by comparing the model results with the observed currents and temperatures at four sites C1, C3, C4 and C5 in LH in 1974–1975 (see Fig. 1). The outer model reproduces reasonably well the general seasonal evolution of the observed sub-surface temperature, but underestimates significantly the observed currents at this site at site C1 located in the deep water of northern LH (not shown). The main reason for the model deficiency at this site may also be associated with the model forcing, particularly the wind forcing discussed earlier.

The outer model performs reasonably well in reproducing the observed sub-surface currents and temperature at 42 m at site C3 (Fig. 15) from day 330 (25 November 1974) to 480 (25 April 1975). In particular, the outer model reproduces reasonably well the typical amplitude and temporal variability of the observed sub-surface currents at this site (Figs. 15(a and b)). However, the nested system reproduces less well the high-frequency variability of the observed sub-surface temperature, and underestimates the observed temperature from day 390–480 at site C3. It should be noted that the nested system is forced by spatially uniform net surface heat flux and LST in which the net heat flux is set to be the seasonal climatology. Therefore, the model performance should be improved significantly if more realistic surface heat flux and LST were to be used.

The model captures reasonably the seasonal evolution of sub-surface temperature (Fig. 16) at 15 m at site C4 located at the southeastern LH. The model underestimates the observed currents, but generates reasonably well the temporal variability of the northward component of the observed currents at this site. At site C5 located at the coastal area of

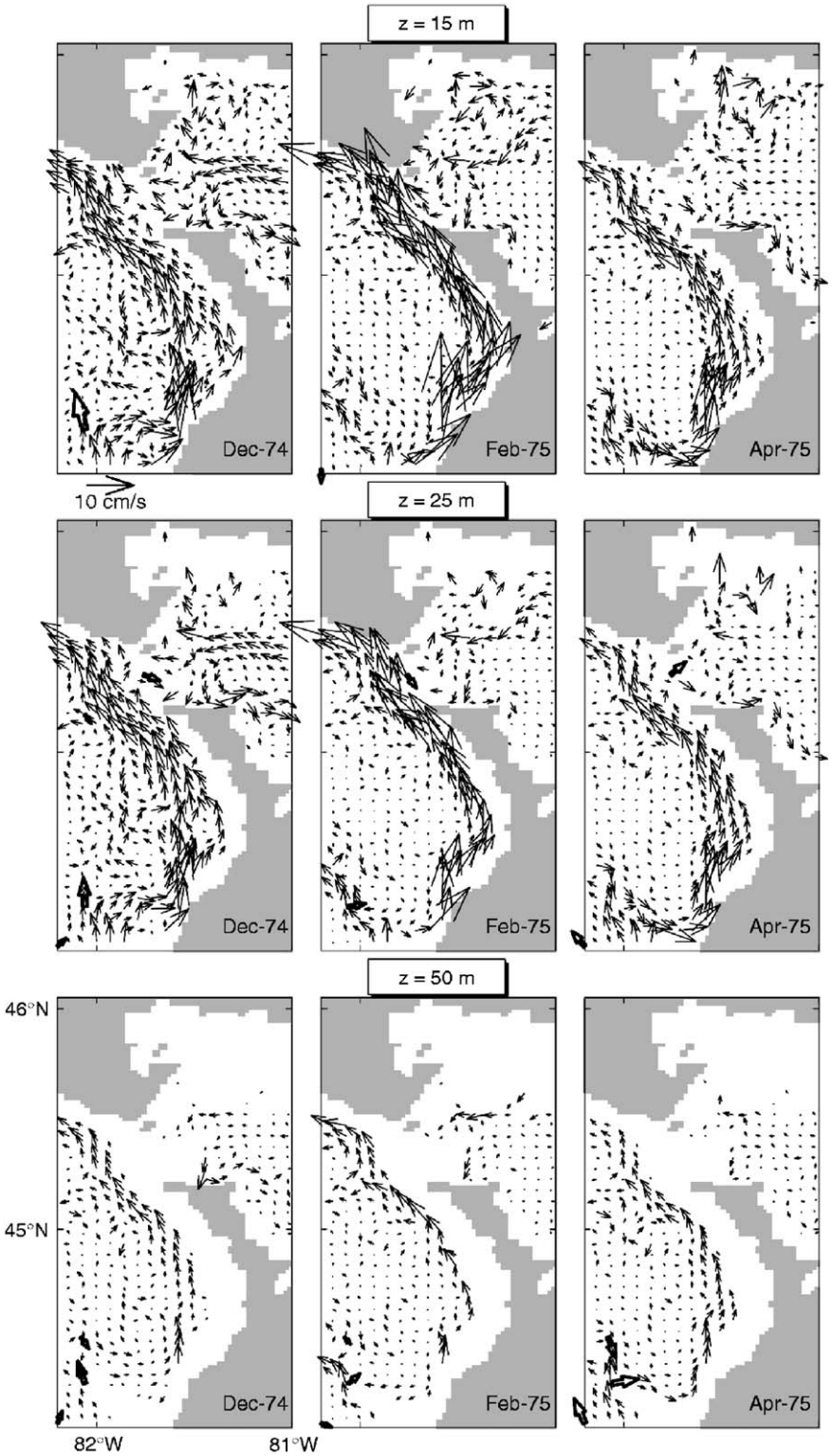


Fig. 14. Comparison of simulated (black arrows) and observed (open arrows) monthly mean currents in 3 months from 3 months of December (1974), February and April (1975) at depths of 15, 25, and 50 m, respectively. The simulated currents are produced by the fine-resolution inner model. Velocity vectors of calculated currents are plotted at every sixth model grid point for clarity.

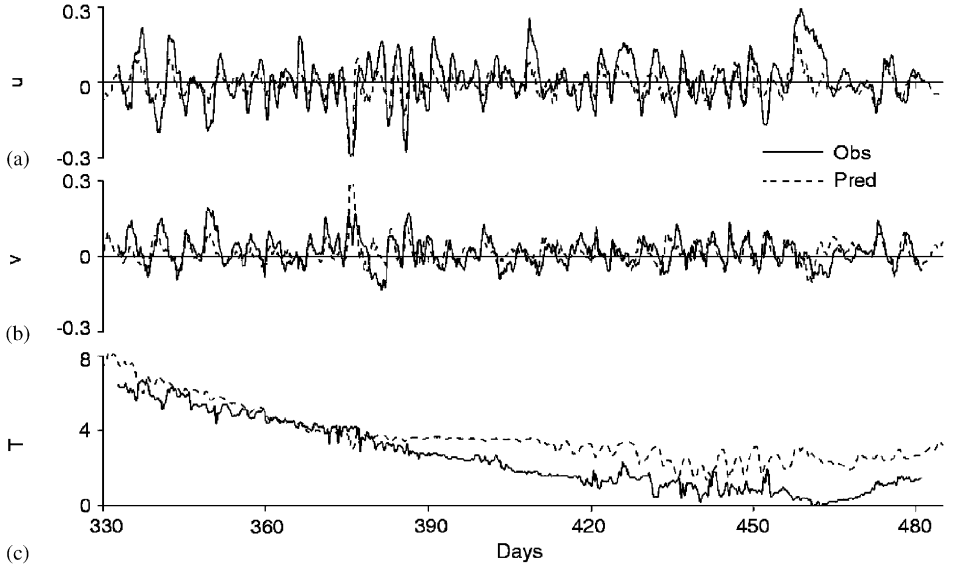


Fig. 15. Time series of simulated (solid) and observed (dashed) currents at 42 m at site C3 in years 1974–1975.

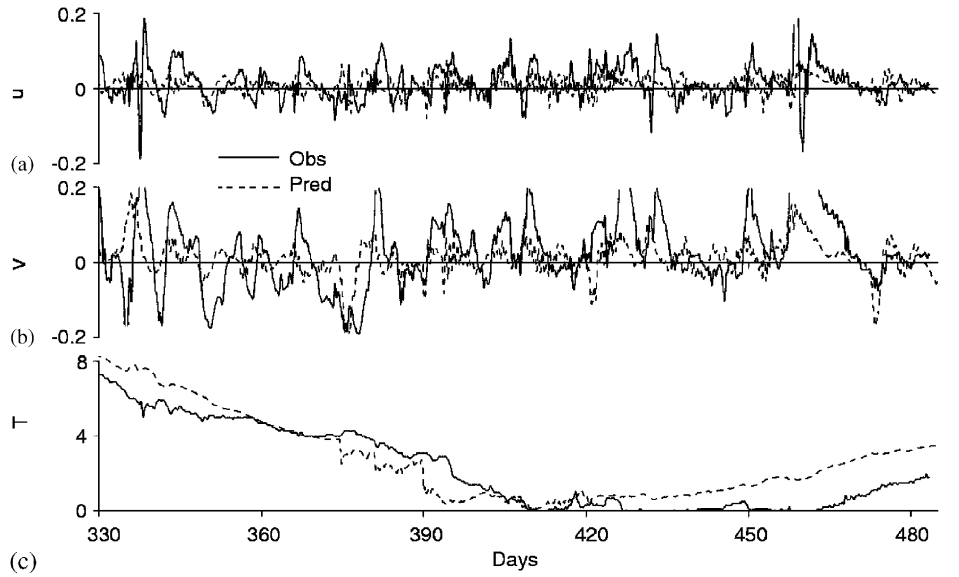


Fig. 16. Time series of simulated (solid) and observed (dashed) currents at 15 m at site C4 in years 1974–1975.

the eastern Main Lake, the simulated currents have similar amplitudes as the observed currents, but have large differences in temporal variability from the observed currents (not shown).

## 5. Summary and conclusion

A nested-grid modelling system was developed for Lake Huron (LH) and Georgian Bay (GB) based on the primitive equation $z$-level ocean circulation model known as CANDIE. We used this nested-grid modelling system to reconstruct the large-scale circulation and temperature distributions in 1974–1975. During this period an extensive field program was conducted in LH. Saylor and Miller (1979) examined the monthly mean circulation and thermal structure in LH from the observations during this period. Numerical studies of the three-dimensional circulation and thermal structure in LH during this period, however, were not made. The

present study was the first attempt to apply a nested-grid modelling system to simulate the 3D circulation and thermal distributions in LH and GB and validate the model performance using the current and temperature observations made in the lake in 1974–1975.

We forced the model with monthly mean net heat flux and 12 hourly wind stress calculated from the wind speeds extracted from the coarse-resolution NCEP/NCAR reanalysis data with amplitudes modified based on the observed wind in the lake. The observed lake surface temperature was also used in forcing the model. The model results generate a cyclonic coastal jet in both LH and GB, which is relatively stronger in summer and fall than those in other seasons. The model also generates reasonably well the seasonal evolution of thermal stratifications in the upper 30 m in the lake. The fine-resolution inner model simulates reasonably well the three-dimensional circulation and thermal structures over the coastal boundary layer close to the eastern shore of LH. A comparison of model results with the observed currents and temperature fields demonstrates significant skills of the $z$-level CANDIE model in simulating the large-scale hydrodynamics in LH and GB and fine-scale circulation over the coastal region.

Although the NCEP/NCAR reanalysis data combined with limited observed winds yielded reasonable estimates of currents and temperature in the lake, there are many areas for further improvement. One of such areas is to have a better horizontal resolution of wind forcing and surface heat flux derived from a meso-scale atmospheric model. As observed in sigma-level models (Beletsky and Schwab, 2001), our numerical results also show a somewhat shallow mixed layer and a diffused thermocline. With improved vertical resolution and better meteorological forcing the numerical model results can be further improved. Most importantly, large shallow portions of LH are covered by ice during the winter. Although it is beyond the scope of this study, the future modelling studies of LH should include an ice model coupled to the 3D hydrodynamic model. Finally, the principal reason for developing LH hydrodynamic model is to use the circulation patterns predicted by the circulation model to better estimate the transport of suspended and dissolved chemical and biological material that can affect the water quality. Some studies in this direction are already in progress.

## Acknowledgements

The authors wish to thank Jiuxing Xing, Alan Davies, Richard Greatbatch and two anonymous reviewers for their very useful comments and suggestions. This project was supported by a contract from Environment Canada. JS is also supported by the NSERC/MARTEC/MSC Industrial Research Chair, and R.Y. is supported by Aquaculture Fund.

## Appendix A. Basic equations of the ocean circulation model

The three-dimensional ocean circulation model known as CANDIE (http://www.phys.ocean.dal.ca/programs/CANDIE, or see Sheng et al. (1998, 2001) is used in this study. The governing equations of the model can be written in spherical coordinates as

$$\frac{\partial u}{\partial t}+Lu-\left(f+\frac{u\tan\phi}{R}\right)v=-\frac{1}{\rho_0 R\cos\phi}\frac{\partial p}{\partial\lambda}+D_{\mathrm{m}}u+\frac{\partial}{\partial z}\left(K_{\mathrm{m}}\frac{\partial u}{\partial t}\right),$$

$$\frac{\partial v}{\partial t}+Lv+\left(f+\frac{u\tan\phi}{R}\right)u=\frac{1}{\rho_0 R}\frac{\partial p}{\partial\phi}+D_{\mathrm{m}}v+\frac{\partial}{\partial z}\left(K_m\frac{\partial v}{\partial z}\right),$$

$$\frac{\partial p}{\partial z}=-\rho g,$$

$$\frac{1}{R\cos\phi}\left(\frac{\partial u}{\partial\lambda}+\frac{\partial(v\cos\phi)}{\partial\phi}\right)+\frac{\partial w}{\partial z}=0,$$

$$\rho=\rho(T,S,p),$$

$$\frac{\partial T}{\partial t}+LT=D_{\mathrm{h}}T+\frac{\partial}{\partial z}\left(K_h\frac{\partial T}{\partial z}\right),$$

$$\frac{\partial S}{\partial t}+LS=D_{\mathrm{h}}S+\frac{\partial}{\partial z}\left(K_h\frac{\partial S}{\partial z}\right),$$

$$L_q=\frac{1}{R\cos\phi}\frac{\partial(uq)}{\partial\lambda}+\frac{1}{R\cos\phi}\frac{\partial(\cos\phi vq)}{\partial\phi}+\frac{\partial(wq)}{\partial z},$$

$$D_{(\mathrm{m,h})}q=\frac{1}{R^2}\left[\frac{1}{\cos^2\phi}\frac{\partial}{\partial\lambda}\left(A_{(\mathrm{m,h})}\frac{\partial q}{\partial\lambda}\right)+\frac{\partial}{\partial\phi}\left(\cos\phi A_{(\mathrm{m,n})}\frac{\partial q}{\partial\phi}\right)\right],$$

where $u$, $v$ and $w$ are the east, north and vertical components of the flow, $p$ is pressure, and $\rho$ is the density calculated from the model potential

temperature $T$ and salinity $S$ which, in turn, are updated using the conservation equations. Here $K_m$ and $K_h$ are vertical eddy viscosity and diffusivity coefficients, $f$ is the Coriolis parameter, $\rho_0$ is a reference density, $R$ and $g$ are the Earth's radius and gravitation acceleration, $L$ is an advection operator, $D_m$ and $D_h$ are diffusion operators, and $A_m$ and $A_h$ are horizontal eddy viscosity and diffusivity coefficients, respectively.

## References


Adcroft, A., Hill, C., Marshall, J., 1997. Representation of topography by shaved cells in a height coordinate ocean model. Monthly Weather Review 2293–2315.

Beletsky, D., O'Connor, W.P., Schwab, D.J., Dietrich, D.E., 1997. Numerical simulation of internal Kelvin waves and coastal upwelling fronts. Journal of Physical Oceanography 27, 1197–1215.

Beletsky, D., Schwab, D.J., 2001. Modeling circulation and thermal structure in Lake Michigan: annual cycle and interannual variability. Journal of Geophysical Research 106, 19745–19771.

Beletsky, D., Saylor, J.H., Schwab, D.J., 1999. Mean circulation in the Great Lakes. Journal of Great Lakes Research 25, 78–93.

Boyce, F.M., Donelan, M.A., Hamblin, P.F., Murthy, C., Simons, T., 1989. Thermal structure and circulation in the Great Lakes. Atmosphere-Ocean 27, 607–642.

Csanady, G.T., 1968. Motions in a model great lake due to a suddenly imposed wind. Journal of Geophysical Research 73, 6435–6447.

Csanady, G.T., 1971. Baroclinic boundary currents and edge waves in basins with sloping shore. Journal of Physical Oceangraphy 1, 92–104.

Csanady, G.T., 1972a. Response of large stratified lakes to wind. Journal of Physical Oceangraphy 2, 3–13.

Csanady, G.T., 1972b. The coastal boundary layer in Lake Ontario. Part I: the spring regime. Journal of Physical Oceangraphy 2, 13–41.

Davidson, F., Greatbatch, R.J., Goulding, A.D., 1998. On the net cyclonic circulation in large stratified lakes. Journal of Physical Oceangraphy 28, 527–534.

Davidson, F., Greatbatch, R.J., deYoung, B., 2001. Asymmetry in the response of a stratified coastal embayment to wind forcing. Journal of Geophysical Research 106, 7001–7016.

Dietrich, D.E., 1997. Application of a modified Arakawa 'a' grid ocean model having reduced numerical dispersion to the Gulf of Mexico circulation. Dynamics of Atmosphere and Oceans 27, 201–217.

Durski, S.M., Glenn, S.M., Haidvogel, D.B., 2004. Vertical mixing schemes in the coastal ocean: Comparison of the level 2.5 Mellor-Yamada scheme with an enhanced version of the K profile parameterization. Journal of Geophysical Research 109, C01015.

Haney, R.L., 1971. Surface thermal boundary conditions for ocean circulation models. Journal of Physical Oceanography 1, 241–248.

Harrington, M.W., 1894. Currents of the Great Lakes as Deduced from the Movements of Bottle Papers During the Seasons of 1892 and 1893. US Weather Bureau, Washington, DC.

International Joint Commission (IJC), 1977. The waters of Lake Huron and Lake Superior. vol. III (Part B), Lake Superior, Windsor, Ontario.

Kalnay, E., et al., 1996. The NCEP/NCAR 40-year reanalysis project. Bulletin of the American Meteorological Society 77, 437–472.

Killworth, P.D., Edwards, N.R., 1999. A turbulent bottom boundary layer code for use in numerical ocean models. Journal of Physical Oceanography 29, 1221–1238.

Large, W.G., Pond, S., 1981. Open ocean momentum flux measurements in moderate to strong winds. Journal of Physical Oceanography 11, 324–336.

Large, W.G., McWilliams, J.C., Doney, S.C., 1994. Oceanic vertical mixing: a review and a model with a nonlocal boundary layer parameterization. Reviews of Geophysics 32, 363–403.

Lu, Y., Thompson, K.R., Wright, D.G., 2001. Tidal currents and mixing in the Gulf of St. Lawrence: an application of the incremental approach to data assimilation. Canadian Journal of Fisheries and Aquatic Sciences 58, 723–735.

Mellor, G.L., Yamada, T., 1982. Development of a turbulence closure model for geophysical fluid problems. Review of Geophysical and Space Physics 20, 851–875.

Murthy, C.R., Dunbar, D.S., 1981. Structure of the flow within the coastal boundary layer of the Great Lakes. Journal of Physical Oceanography 11, 1567–1577.

Rao, Y.R., Murthy, C.R., 2001. Coastal boundary layer characteristics during summer stratification in Lake Ontario. Journal of Physical Oceanography 31, 1088–1104.

Saylor, J.H., Miller, G.S., 1979. Lake Huron winter circulation. Journal of Geophysical Research 84, 3237–3252.

Schwab, D.J., Bedford, K.W., 1994. Initial implementation of the Great Lakes forecasting system: A real-time system for predicting lake circulation and thermal structure. Water Pollution Research Journal Canada 29, 203–220.

Schwab, D.J., Beletsky, D., 2003. Relative effects of wind stress curl, topography, and stratification on large-scale circulation in Lake Michigan. Journal of Geophysical Research 108, 3044.

Schwab, D.J., Sellers, D.L., 1996. Computerized bathymetry and shorelines of the Great Lakes. *NOAA report, ERL GLERL-16, GLERL*, Ann Arbor, MI, USA.

Shchepetkin, A.F., McWilliams, J.C., 2003. A method for computing horizontal pressure-gradient force in an ocean model with a non-aligned vertical coordinate, Journal of Geophysical Research 108, C3090.

Sheng, J., 2001. Dynamics of a buoyancy-driven coastal jet: The Gaspe Current. Journal of Physical Oceanography 31, 3146–3162.

Sheng, J., Tang, L., 2003. Numerical studies of circulation in the western Caribbean Sea. Journal of Physical Oceanography 33, 2049–2069.

Sheng, J., Tang, L., 2004. A two-way nested-grid ocean-circulation model for the Meso-American Barrier Reef System. Ocean Dynamics 52, 232–242.

Sheng, J., Wang, L., 2004. Numerical study of tidal circulation and nonlinear dynamics in Lunenburg Bay, Nova Scotia. Journal of Geophysical Research 109, C10018.

Sheng, J., Greatbatch, R.J., Wright, D.G., 2001. Improving the utility of ocean circulation models through adjustment of the momentum balance. Journal of Geophysical Research 106, 16711–16728.

Sheng, J., Greatbatch, R.J., Zhai, X., Tang, L., 2005. A new two-way nesting technique based on the smoothed semi-prognostic method. Ocean Dynamics 55, 162–177.

Sheng, J., Wright, D.G., Greatbatch, R.J., Dietrich, D., 1998. CANDIE: a new version of the DieCAST ocean circulation model. Journal of Atmospheric and Oceanic Technology 15, 1414–1432.

Simons, T.J., 1974. Verification of numerical models of Lake Ontario: part I. Circulation in spring and early summer. Journal of Physical Oceanography 4, 507–523.

Sloss, P.W., Saylor, J.H., 1975. Measurement of current flow during summer in Lake Huron. NOAA Technical Report ERL 353 GLERL 5. US Department of Commerce, Boulder, CO.

Smagorinsky, J., 1963. General circulation experiments with the primitive equation I. The basic experiment. Monthly Weather Review 21, 99–165.

Song, Y.T., 1998. A general pressure gradient formulation for ocean model. I. Scheme design and diagnostic analysis. Monthly Weather Review 126, 3213–3230.

Song, Y.T., Chao, Y., 2000. An embedded bottom boundary layer formulation for z-coordinate ocean models. Journal of Atmospheric Oceanic Technology 17, 546–560.

Thuburn, J., 1996. Multidimensional flux-limited advection schemes. Journal of Computational Physics 123, 74–83.

Wang, L., Sheng, J., Hay, A.E., Schillinger, D., 2006. Storm-induced circulation in Lunenburg Bay of Nova Scotia: observations and numerical simulations. *Journal of Physical Oceanography*, in press.

Xing, J., Davies, A.M., 1995. Application of three-dimensional models to the determination of tidal mixing and currents in a shallow sea. Progress in Oceanography 35, 153–205.

Xing, J., Davies, A.M., 2001. A three-dimensional baroclinic model of the Irish Sea: formation of the thermal fronts and associated circulation, multidimensional flux-limited advection schemes. Journal of Physical Oceangraphy 31, 94–114.